Mucosal Immunology xxx (xxxx) xxx

Contents lists available at ScienceDirect

Mucosal Immunology

journal homepage: www.elsevier.com/mi

Article

TIFA renders intestinal epithelial cells responsive to microbial ADP-heptose and drives colonic inflammation in mice

Lena Erkert [a], Barbara Ruder [a,1], Melanie Kabisch [a], Reyes Gamez Belmonte [a], Jay V. Patankar [a,b], Miguel Gonzalez Acera [a], Lena Schödel [a], Mircea T. Chiriac [a], Roodline Cineus [c], Stylianos Gnafakis [d], Tamara Leupold [a], Oana-Maria Thoma [a,b], Iris Stolzer [a], Astrid Taut [a], Veronika Thonn [a], Sebastian Zundler [a,b], Claudia Günther [a,b], Andreas Diefenbach [d], Anja A. Kühl [e], Ahmed N. Hegazy [c,f], Maximilian Waldner [a,b], Marijana Basic [g], André Bleich [g], Markus F. Neurath [a,b], Stefan Wirtz [a,b], Christoph Becker [a,b,*], The TRR241 IBDome Consortium

[a] Department of Medicine 1, Universitätsklinikum Erlangen, Friedrich-Alexander-Universität Erlangen-Nürnberg, Germany
[b] Deutsches Zentrum Immuntherapie (DZI), Erlangen, Germany
[c] Department of Gastroenterology, Infectiology and Rheumatology, Charité Universitätsmedizin Berlin, Germany
[d] Department of Microbiology, Infectious Diseases and Immunology, Charité-Universitätsmedizin Berlin, Germany
[e] iPATH.Berlin, Campus Benjamin Franklin, Charité - Universitätsmedizin Berlin, Corporate Member of Freie Universität Berlin, Humboldt-Universität zu Berlin, Berlin, Germany
[f] Deutsches Rheumaforschungszentrum Berlin (DRFZ), an Institute of the Leibniz Association, Berlin, Germany
[g] Institute for Laboratory Animal Science, Hannover Medical School, Hannover, Germany

ARTICLE INFO

Keywords:
TIFA
Intestinal epithelium
IBD
ADP-heptose
IL-22

ABSTRACT

Intestinal immune homeostasis relies on intestinal epithelial cells (IECs), which provide an efficient barrier, and warrant a state of tolerance between the microbiome and the mucosal immune system. Thus, proper epithelial microbial sensing and handling of microbes is key to preventing excessive immunity, such as seen in patients with inflammatory bowel disease (IBD). To date, the molecular underpinnings of these processes remain incompletely understood. This study identifies TIFA as a driver of intestinal inflammation and an epithelial signaling hub between the microbiome and mucosal immune cells. TIFA was constitutively expressed in crypt epithelial cells and was highly induced in the intestine of mice and IBD patients with intestinal inflammation. We further identified IL-22 signaling via STAT3 as key mechanism driving TIFA expression in IECs. At the molecular level, we demonstrate that TIFA expression is essential for IEC responsiveness to the bacterial metabolite ADP-heptose. Most importantly, ADP-heptose-induced TIFA signaling orchestrates an inflammatory cellular response in the epithelium, with NF-κB and inflammasome activation, and high levels of chemokine production. Finally, mice lacking TIFA were protected from intestinal inflammation when subjected to a model of experimental colitis. In conclusion, our study implicates that targeting TIFA may be a strategy for future IBD therapy.

Summary

TIFA in intestinal epithelial cells is essential for the response to microbial ADP-heptose. TIFA is induced by the IL-22-STAT3 pathway, and elevated TIFA levels were detected in IBD. TIFA drives NF-κB activation and the expression of proinflammatory genes.

Introduction

Intestinal epithelial cells (IECs) are key regulators of intestinal immune homeostasis and their dysregulation can lead to inflammation.[1] IECs form a robust barrier which is vital for host defense by creating a physical and biochemical blockade against bacteria in the gut lumen.

* Corresponding author at: Department of Medicine 1, Friedrich-Alexander-University Erlangen-Nürnberg, Erlangen, Germany.
E-mail address: christoph.becker@uk-erlangen.de (C. Becker).
[1] Current affiliation: Research Management and Services, Paracelsus Medical University Nuremberg, Germany.

https://doi.org/10.1016/j.mucimm.2025.01.003
Received 10 June 2024; Accepted 2 January 2025
Available online 20 January 2025

Moreover, IECs are responsible for microbial sensing and handling of microbial products, and the appropriate cellular response, which is then relayed to immune cells in the lamina propria. The gut epithelium negotiates between the microbes in the lumen and the immune cells by selectively allowing beneficial microbial interactions while activating immune responses to pathogenic threats, thus maintaining a balanced intestinal environment. Microbial recognition at the epithelial surface relies on expression of pattern recognition receptors (PRRs) in IECs, including toll-like receptors (TLRs), NOD-like receptors (NLRs) and RIG-I-like receptors (RLRs).[2] These receptors are expressed on the cell surface and in the cytoplasm and recognize various microbe-associated molecular patterns (MAMPs), such as lipopolysaccharide (LPS). Activation of the PRRs leads to a pro-inflammatory response via various downstream signaling cascades, such as NF-κB signaling, MAPK signaling or inflammasome signaling.[3] Thus, it is not surprising that PRR dysfunction is associated with chronic intestinal inflammation, such as inflammatory bowel disease (IBD).[2].

Recently, ADP-*glycero*-β-D-*manno*-heptose (ADP-heptose) was discovered as a novel class of MAMP.[4] ADP-heptose is produced as a soluble intermediate in the lipopolysaccharide biosynthesis of certain pathogenic bacteria. In gastric epithelial cells, ADP-heptose released by *H. pylori* can freely cross the host cell membrane where it is detected by the cytoplasmic PRR Alpha-protein kinase 1 (ALPK1).[5] ALPK1 has been demonstrated to phosphorylate the molecule TRAF-interacting protein with FHA domain-containing protein A (TIFA). Phosphorylation of TIFA leads to oligomerization of TIFA proteins and the formation of so-called TIFAsomes, higher-order multiprotein structures consisting of several cellular proteins including TRAF6 and other important regulators of transcription.[5] TIFA, in turn, can stimulate the oligomerization and polyubiquitination of TRAF6, leading to the activation of TAK1 and the IκB kinase (IKK) complex through a proteasome-independent mechanism.[4–7] Moreover, TIFA might be involved in oxidative stress, inflammasome activation, and tumorigenesis.[8–9] .

In this study, we identified TIFA in IECs as a key mediator of *trans*-epithelial signaling and the host response to microbial ADP-heptose in the context of IBD. TIFA was constitutively expressed in intestinal crypts of the small and large intestine and its expression was highly upregulated during experimental intestinal inflammation and infection in mice and in IBD patient samples. We further provide evidence that TIFA expression is strongly induced in IECs upon IL-22 stimulation, in a strictly STAT3-dependent manner. We also show that TIFA expression is a prerequisite for ADP-heptose signaling in IECs and that TIFA induces a profound pro-inflammatory cellular response characterized by a broad induction of chemokines and cytokines, inflammatory mediators, and inflammasome activation. On a molecular level, TIFA activation is a strong activator of both the canonical and non-canonical NF-κB pathway in IECs. Most importantly, we show that mice lacking TIFA are protected from experimental colitis, suggesting that TIFA is a driver of gut inflammation. In summary, our data reveal a novel, previously unexplored, microbial-epithelial-immune cell crosstalk in IECs, with TIFA as a central regulator, critically involved in intestinal inflammation. Collectively, these results suggest that TIFA may serve as a potential therapeutic target in gut infection and inflammation.

Results and discussion

TIFA is expressed in intestinal crypts and induced during infection and inflammation

Although microbial signaling networks are considered key to the pathogenesis of IBD, their role in disease pathogenesis is still not fully understood. To uncover previously unknown microbial mechanisms driving intestinal inflammation, we applied a heuristic approach by first comparing transcriptomic changes in DSS-treated mice at the peak of inflammation and after complete resolution of inflammation with different murine intestinal infection models that also show inflammatory signatures, such as *H. hepaticus* (+anti-IL10R), *C. rodentium* and *E. vermiformis* infection. While each disease model had a unique transcriptomic signature, the expression of 213 genes was altered in all models tested (Fig. 1**A; left**). Using gene ontology analysis, biological processes such as 'immune response', 'defense response', and 'regulation of immune system processes' were the top pathways affected in this comparison (Fig. 1**A; middle**). By comparing the genes contained in these pathways, a list of 47 overlapping genes was obtained (Fig. 1**A; right,** Suppl. Tab. 1). Among the 47 genes, our approach identified many previously reported IBD-related susceptibility genes, including *Nod2*, *Il10* and *Il1b*. Interestingly, amongst the 10 most significantly regulated genes, we identified *Tifa*, a molecule that has recently been described as a host factor of bacterial heptose recognition,[10] but has so far not been studied in the gut epithelium or linked to IBD pathogenesis. Using fluorescence *in situ* hybridization (FISH) staining, we identified constitutive *Tifa* mRNA expression in epithelial cells of the lower crypt of both the small and large intestine (Fig. 1**B**). Further analysis of a publicly available single-cell RNA sequencing dataset of mouse small intestinal (Si) epithelial cells under basal conditions[11] supported our findings, showing constitutive *Tifa* expression in the stem cell and transit-amplifying fractions, as well as in Paneth cells, cell types located in the lower crypt (Fig. 1**C**). In contrast to the steady-state gut, in the inflamed intestine of mice with experimental colitis or in mice infected with *C. rodentium*, *H. hepaticus* (+anti-IL10R) or *S. typhimurium*, *Tifa* mRNA expression was strongly upregulated in IECs (Fig. 1**D**), a finding further confirmed by qPCR analysis of DSS-treated, *C. rodentium* and *S. typhimurium* infected animals (**Suppl**. Fig. 1A). Noteworthy, in inflamed gut samples, *Tifa* mRNA expression extended far up the crypt, with occasional expression also appearing in the surface epithelium (Fig. 1**D; white arrows**). Further analysis of *Tifa* gene expression throughout the course of DSS-induced colitis in mice revealed an upregulation of *Tifa* already during the onset of intestinal inflammation. *Tifa* expression remained high during the peak of inflammation and rapidly decreased to steady-state levels during the resolution process (Fig. 1**E**). Interestingly, in both CD and UC gut samples, we observed a significantly higher *TIFA* expression than in healthy individuals, suggesting that TIFA may play a role in the pathogenesis of IBD (Fig. 1**F;** Suppl. Tab. 2). Interestingly, in inflamed areas of CD and UC patients, TIFA was observed to form aggregates within the cytoplasm of IECs (Fig. 1**G, arrows**), which may imply the presence of TIFAsome formation and thus suggests activation of the TIFA signaling pathway in IBD. Furthermore, correlation analysis between *TIFA* expression and histopathologic scoring revealed a moderate positive correlation, which was further supported by a strong positive correlation between *TIFA* expression and the pro-inflammatory marker *NOS2* in colon samples from IBD patients (Fig. 1**H**).

Intestinal epithelial TIFA is induced by IL-22 signaling in a STAT3-dependent manner

Our initial analyses of TIFA expression in the gut revealed constitutive expression in the lower crypt and an inducible expression in the whole epithelium during inflammatory or infectious challenges. This suggested that epithelial TIFA expression is regulated, at least in part, by the local immune cell microenvironment. In support of this assumption, *Tifa* expression was detected in freshly isolated IECs but not in Si organoids cultured *in vitro* for 10 days (Fig. 2**A**). Germ-free mice exhibited reduced, but not abolished, *Tifa* mRNA expression levels, as shown by staining of the ileum of germ-free mice (**Suppl**. Fig. 1**B**) and RNA sequencing analysis of colon samples from these mice (**Suppl**. Fig. 1**C**) compared to conventional specific pathogen-free (SPF) mice. In an approach to identify signals that drive inflammation-induced *Tifa* expression in IECs, we stimulated intestinal organoids from wild-type animals with supernatants of T cell cultures polarized to different effector lineages. Interestingly, while supernatants of Th0, Th1, Th2, or regulatory T (Treg) cell cultures had little effect on *Tifa* expression,

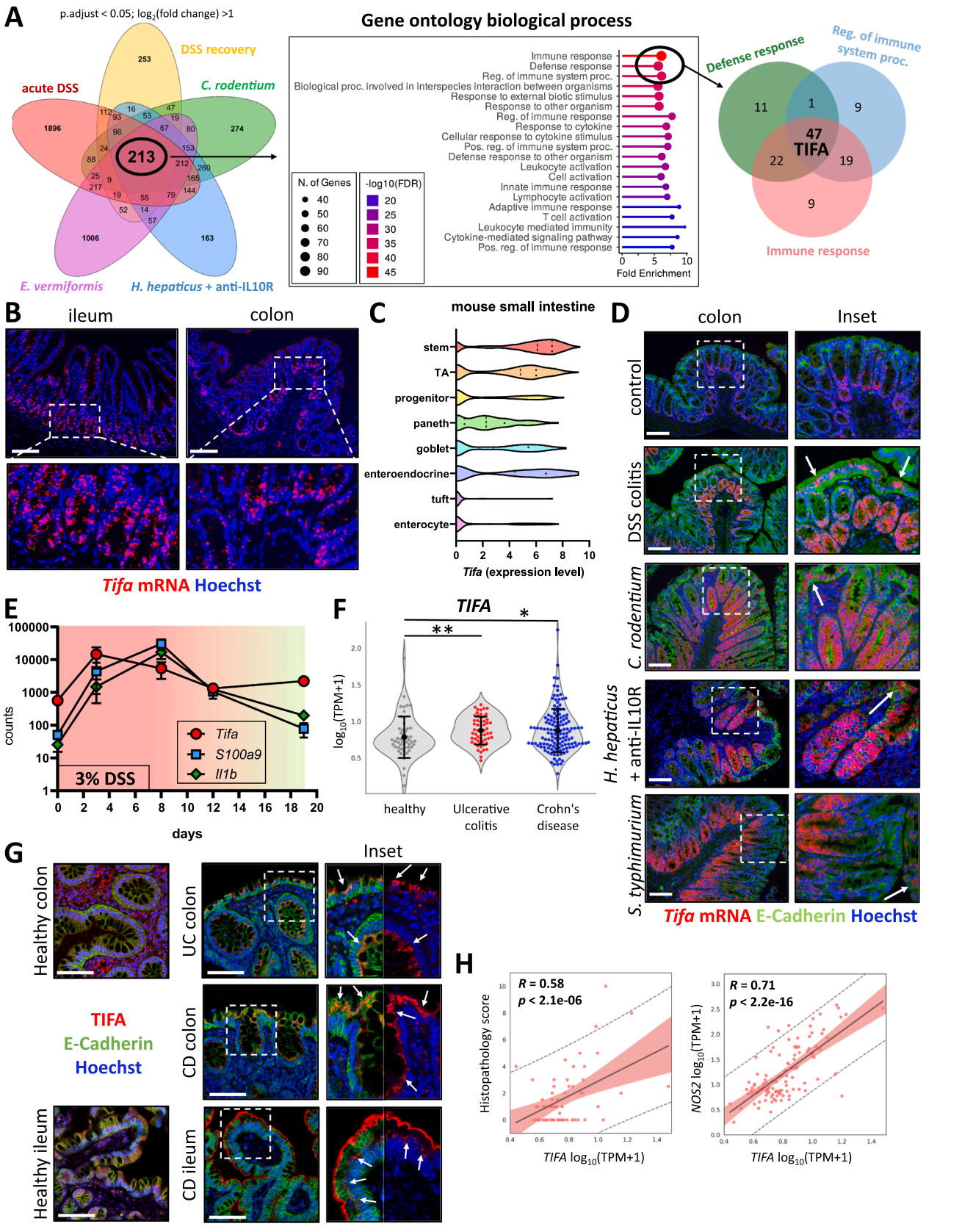

(caption on next page)

Fig. 1. TIFA is induced during intestinal infection and inflammation and is upregulated in IBD. **(A, left)** Venn diagram of RNA sequencing data from colonic tissues of DSS-treated mice at the peak of inflammation or after full recovery, as well as mice infected with *Helicobacter hepaticus* (+anti-IL10R), *Citrobacter rodentium* or *Eimeria vermiformis*. Only genes with an adjusted p-value < 0.05 and a $\log_2$(fold change) > 1 were considered (n = 3/group). **(A, middle)** Enriched gene ontology biological processes (GO_BP) terms of the 213 overlapping genes from (A, left). **(A, right)** Venn diagram of the genes obtained from the gene ontology biological process pathways 'immune response', 'defense response', and 'regulation of immune system process' shown in (A, middle). **(B)** Representative fluorescence *in situ* hybridization staining images of *Tifa* mRNA in the murine ileum and colon (scale bar 100 μm) (3 independent experiments; n = 8/group). **(C)** *Tifa* expression levels in murine small intestinal epithelial cells, analyzed from a publicly available dataset[11]. **(D)** Representative images of *Tifa* mRNA (red) and E-Cadherin (green) expression in colonic tissue from mice treated with DSS or infected with *Citrobacter rodentium*, *Helicobacter hepaticus* (+ anti-IL10R), or *Salmonella typhimurium* (scale bar 100 μm) (n ≥ 3/group: DSS: 8; *Citrobacter*: 6; *Hepaticus*: 6; *Salmonella*: 4) with *Tifa* mRNA expression observed in the surface epithelium (white arrows). **(E)** *Tifa*, *S100a9*, and *Il1b* normalized counts in different inflammatory stages of DSS-induced colitis in mice (n = 2–3/group), analyzed from a publicly available dataset[34]. **(F)** *TIFA* gene expression in patients with Crohn's disease and Ulcerative colitis compared to healthy controls (healthy control: n = 52; CD: n = 57; UC: n = 92). **(G)** Representative immunofluorescence staining images of TIFA (red) counterstained with E-Cadherin (green) as an epithelial marker in inflamed tissues of Ulcerative colitis (UC) and Crohn's disease (CD) patients compared to healthy individuals (scale bar 100 μm) (healthy: n = 12; UC: n = 7; CD: n = 24). **(H)** Comparison of *TIFA* expression and the histopathologic inflammation score in colon samples from IBD patients versus healthy subjects (left), and comparison between *TIFA* and *NOS2* expression levels (right). Overall, data are presented as mean ± SD. * and ** indicate $p < 0.05$ and $p < 0.01$, respectively, by Wilcoxon-Mann-Whitney test (F, H).

supernatant from Th17 cells strongly increased *Tifa* expression in epithelial organoids (Fig. 2**B**). Direct stimulation of epithelial organoids with Th17-derived cytokines, such as IL-17A, IL-17F, or IL-21, did not affect *Tifa* expression. As previously described for other cell types,[8] TNF-α was able to modestly upregulate *Tifa* in epithelial organoids. In contrast, IL-22 stimulation resulted in a highly significant increase in relative *Tifa* transcript levels (Fig. 2**C**). Analysis of an online available dataset of human epithelial organoids stimulated with IL-22 confirmed this result[12] (Fig. 2**D**). Notably, classical TLR ligands failed to upregulate *Tifa* expression in IECs (**Suppl.** Fig. 1**D**). Thus, our data suggest that TIFA expression is regulated by immune-epithelial rather than by microbial-epithelial signaling. To demonstrate the effect of IL-22 on *Tifa* expression *in vivo*, mice were injected with an IL-22 minicircle expression vector for systemic overexpression[13] (**Suppl**. Fig. 1**E**). Strikingly, mice receiving an IL-22 minicircle vector showed a strongly upregulated *Tifa* mRNA expression throughout the ileal and colonic epithelium compared to mice receiving a control vector (Fig. 2**E**). Conversely, in the absence of IL-22 or its receptor on IECs (using *Il22*$^{-/-}$ and *Il22ra*$^{\Delta IEC}$ mice, respectively) reduced levels of *Tifa* mRNA expression were detected by qPCR analysis and *Tifa* FISH staining (Fig. 2**F** and **G**). However, we still observed some *Tifa* expression in crypt epithelial cells of *Il22*$^{-/-}$ mice (Fig. 2**G**), suggesting additional IL-22-independent pathways of *Tifa* expression *in vivo*, such as those induced by TNF-α signaling. Previous work from our group and others has shown that the effects of IL-22 in IECs during colitis are mediated by STAT3.[14–16] Indeed, IL-22-dependent *Tifa* upregulation was completely abolished in organoids from mice lacking STAT3 in IECs (Fig. 2**H**). Further confirmation of *Tifa* induction via the IL-22-STAT3 axis was obtained *in vivo* in *Stat3*$^{\Delta IEC}$ animals, which showed lower *Tifa* mRNA expression under steady-state conditions than in littermate control animals (Fig. 2**I**). Similar to IL-22-deficient mice, *Tifa* staining was significantly reduced but not completely abolished in these animals. In conclusion, to the best of our knowledge, this is the first report demonstrating that *Tifa* expression is induced by immune-epithelial signaling via the IL-22-STAT3 axis in IECs.

ADP-heptose drives TIFAsome formation and a pro-inflammatory response in intestinal epithelial cells

Previous studies in gastric cells demonstrated that ADP-heptose released by Gram-negative bacteria binds to the recently discovered PRR ALPK1, which in turn can activate TIFA through phosphorylation, leading to NF-κB activation.[5–6] To provide evidence for the activation of TIFA signaling by ADP-heptose, both mouse and human intestinal epithelial organoid monolayer cultures were transfected with a plasmid encoding for a fusion protein of TIFA and the mScarlet2 reporter protein. This approach ensured detectable TIFA expression *in vitro* without the need for IL-22 stimulation to enhance TIFA levels. Notably, recent evidence from gastric cells indicates that activation of TIFA signaling results in the formation of higher-order protein complexes known as TIFAsomes.[5] Strikingly, while in unstimulated monolayers we detected TIFA equally distributed in the cytoplasm, the addition of ADP-heptose to transfected 2D organoid cultures led to the formation of TIFAsomes (Fig. 3**A**). Of note, TIFAsome formation was specifically observed only upon exposure to ADP-heptose, whereas stimulation of these cultures with IL-22 alone did not induce TIFAsome formation (**Suppl**. Fig. 1**F**).

To investigate whether IECs are regulated by ADP-heptose, we first stimulated intestinal organoids from wild-type mice with IL-22 (which is necessary to induce *Tifa* expression) and subsequently with ADP-heptose. When comparing the differential expression of genes (DEG) between Si organoids stimulated with IL-22 alone and those stimulated with IL-22 plus ADP-heptose against Si organoids that were not stimulated, we identified 1118 genes uniquely affected by ADP-heptose stimulation (Fig. 3**B**), indicating that ADP-heptose induces major transcriptomic changes in IECs. Gene ontology (GO) analysis of ADP-heptose induced transcriptomic changes revealed pathways related to bacterial response, such as 'defense response to Gram-positive/-negative bacterium' and 'cellular response to lipopolysaccharide' (Fig. 3**C,** Suppl. Tab. 3). Interestingly, we also identified that ADP-heptose stimulation of organoids resulted in a significant repression of genes for antimicrobial peptides, including various defensins and *Lyz1*, suggesting a negative impact of ADP-heptose signaling on Paneth cells (**Suppl**. Fig. 2**A**). Moreover, the analyses also revealed that ADP-heptose induced a broad inflammatory response in IECs, including pathways related to 'innate immune response in mucosa', 'inflammatory response', and 'regulation of I-kappa kinase/NF-kappaB signaling', but also 'positive regulation of cytokine production', and 'chemotaxis'. A comparison of ADP-heptose-dependent transcriptomic changes in Si organoids from wild-type mice with transcriptomic data from colon tissue samples from highly inflamed DSS-treated wild-type mice revealed a strong positive correlation between the two datasets ($r = 0.81$). In addition to *Tifa* (marked in red) and chemokines (marked in green), genes regulated by NF-κB (marked in blue) were highly upregulated in both datasets, suggesting that IECs exposed to ADP-heptose might contribute to an inflammatory epithelial response (Fig. 3**D**). Induction of pro-inflammatory genes by ADP-heptose was further confirmed in human organoids, which showed upregulation of *CCL20* and *NOS2* upon stimulation (Fig. 3**E**), further supporting a role for the ADP-heptose-ALPK1-TIFA signaling pathway in the human gut epithelium. Of note, to avoid the need for IL-22 stimulation – required for *Tifa* induction *in vitro* – we used murine IECs cultured for only 2 days *in vitro*. These short-term cultures retain *Tifa* expression levels comparable to freshly isolated IECs, enabling us to examine the effects of ADP-heptose stimulation alone. This approach revealed significantly increased expression of the NF-κB target genes *Nos2* and *Ccl9* (**Suppl.** Fig. 2**B**) and higher levels of phospho-p65 as shown by Western blot analysis (**Suppl.** Fig. 2**C**). In agreement with the above-mentioned data, use of the Ingenuity® Pathway Analysis software package (IPA; Qiagen) revealed activation of the NF-κB signaling pathway in ADP-heptose- and lL-22-stimulated wild-type organoids (**Suppl**. Fig. 2**D**), along with predicted activation not only of the NLRP3

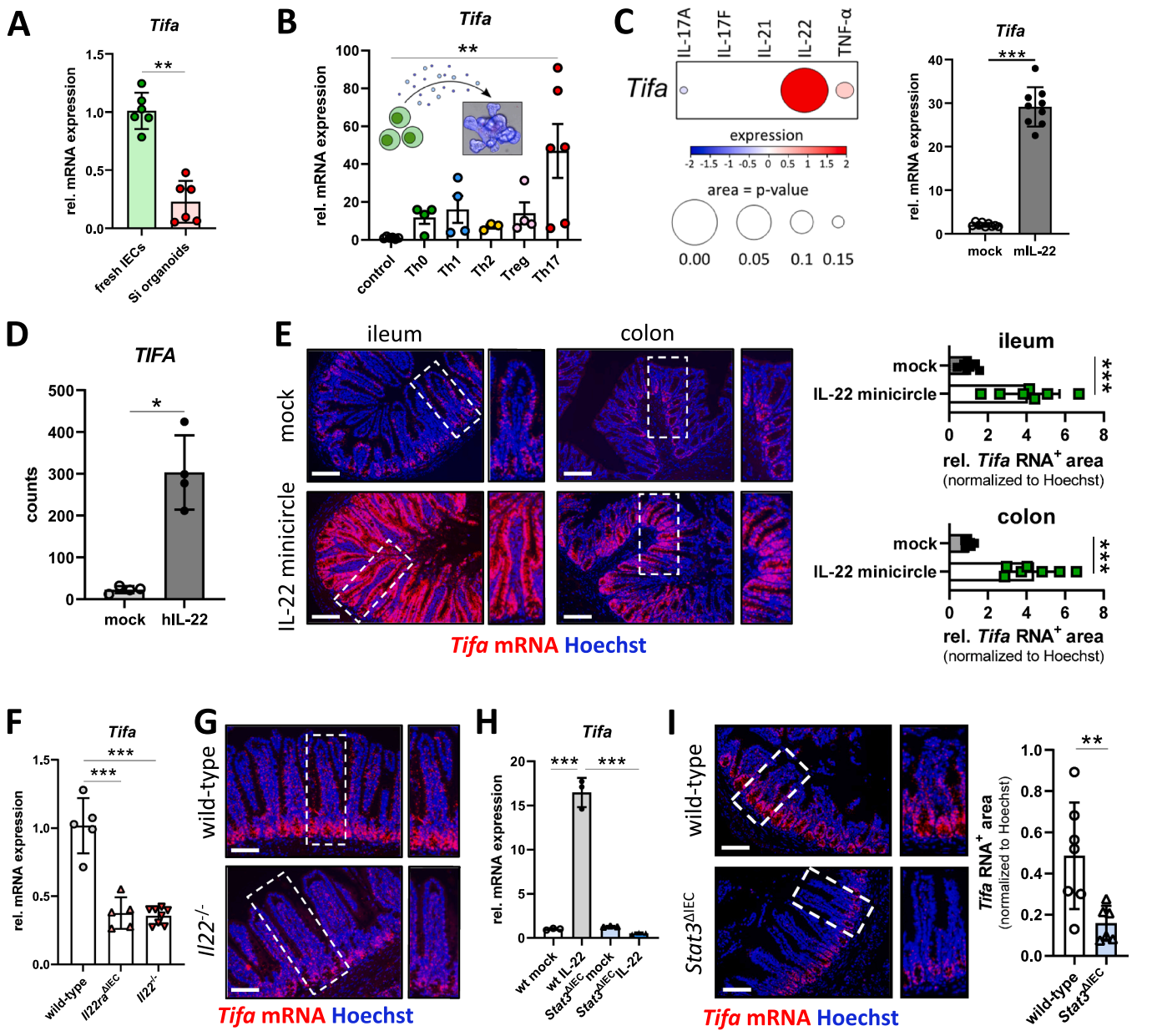

Fig. 2. TIFA is induced by IL-22-STAT3 signaling in the intestinal epithelium. **(A)** *Tifa* mRNA expression in freshly isolated IECs from wild-type mice compared to *Tifa* mRNA expression in wild-type Si organoids (n = 6/group). **(B)** *Tifa* mRNA expression in Si organoids stimulated with polarized T cell supernatants (3 independent experiments; n = 3–6/group). **(C)** Gene expression analysis of *Tifa* in Si organoids stimulated with different cytokines characteristic for Th17 cells (left), and *Tifa* fold-induction of Si organoids stimulated with IL-22 (right) were calculated relative to mock, *Gapdh* was used for normalization (left: n = 3/group; right: 3 independent experiments; n = 9/group). **(D)** *TIFA* expression from an online available dataset of human colonic organoids treated with 10 ng/ml hIL-22 for 24 h. **(E)** Representative FISH staining images of *Tifa* mRNA expression in the ileum and colon of mice injected with an IL-22 minicircle vector (scale bar 100 μm) with measurement of the relative *Tifa* mRNA^{+} area (normalized to Hoechst) (n = 7/group). **(F)** *Tifa* mRNA levels (normalized to *Hprt*) in the ileum of *Il22ra*$^{\Delta IEC}$ and *Il22*$^{-/-}$ mice compared to wild-type (wt) mice (n = 5–8/group). **(G)** Representative FISH staining images of *Tifa* mRNA expression in the ileum of *Il22*$^{-/-}$ mice (scale bar 100 μm) (n = 3–5/group). **(H)** *Tifa* gene expression analysis in wt and *Stat3*$^{\Delta IEC}$ Si organoids stimulated with or without IL-22 (2 independent experiments). **(I)** Representative FISH staining images of *Tifa* mRNA expression in the ileum of wt and *Stat3*$^{\Delta IEC}$ mice (scale bar 100 μm) with measurement of the *Tifa* mRNA^{+} area (normalized to Hoechst) (n = 6–7/group). Overall, data are presented as mean ± SD. *, **, and *** indicate $p < 0.05$, $p < 0.01$, and $p < 0.001$, respectively, by Mann-Whitney test (A, C, D, E, I) or one-way ANOVA (Tukey's post hoc test: B, F, H).

inflammasome, but also of the NLRP1, AIM2, and NLRC4 inflammasomes (Fig. 3**F**). In conclusion, we have demonstrated for the first time that human and mouse primary IECs respond to ADP-heptose with activation of the ALPK1-TIFA signaling pathway and the expression of a wide range of pro-inflammatory genes.

TIFA is essential for the intestinal epithelial cell response to microbial ADP-heptose

To prove that the ADP-heptose-stimulated effects in IECs are indeed TIFA dependent, we stimulated Si organoids from *Tifa*$^{+/+}$ and *Tifa*$^{-/-}$ mice with IL-22 together with or without ADP-heptose and performed RNA sequencing (Fig. 4**A**). Of note, the functional knockout of *Tifa* in these animals was confirmed at the RNA level (**Suppl.** Fig. 3**A** and **B**).

Intriguingly, as depicted in a Principal Component Analysis (PCA), whereas a striking response to ADP-heptose was observed in wildtype-derived organoids, the loss of TIFA in *Tifa*$^{-/-}$ organoids resulted in a completely abolished response to ADP-heptose in IECs (Fig. 4**B**). In particular, ADP-heptose treatment induced 1329 DEG in wild-type organoids, while TIFA-deficient organoids exposed to ADP-heptose did not show any DEG. On the other hand, in the absence of ADP-heptose, no major transcriptomic differences were observed between TIFA-

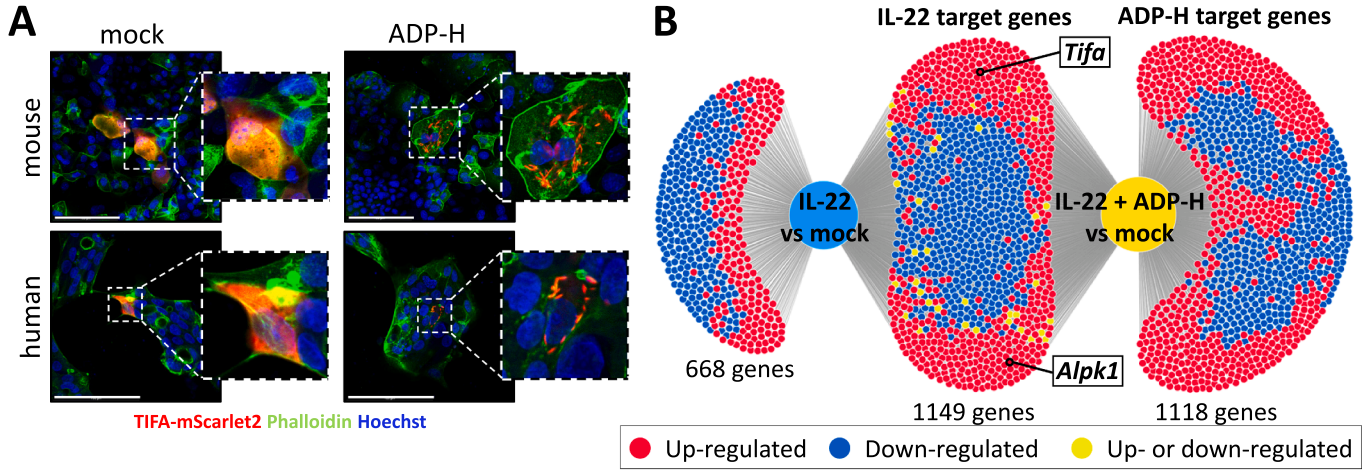

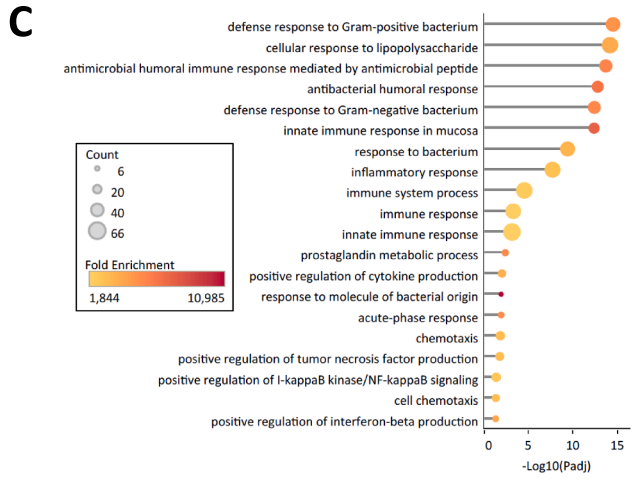

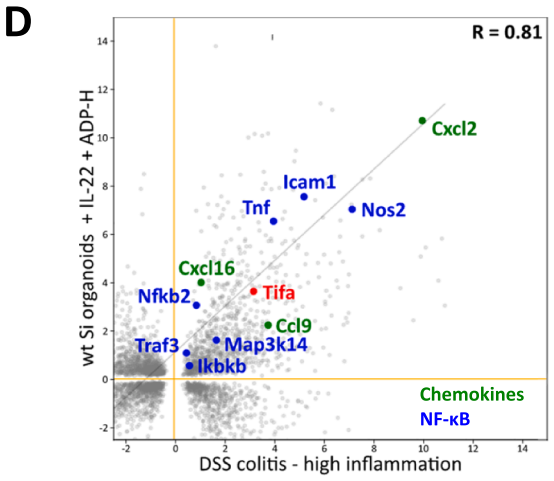

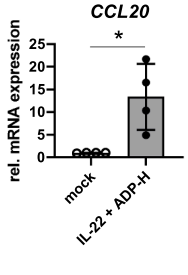

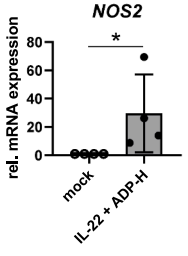

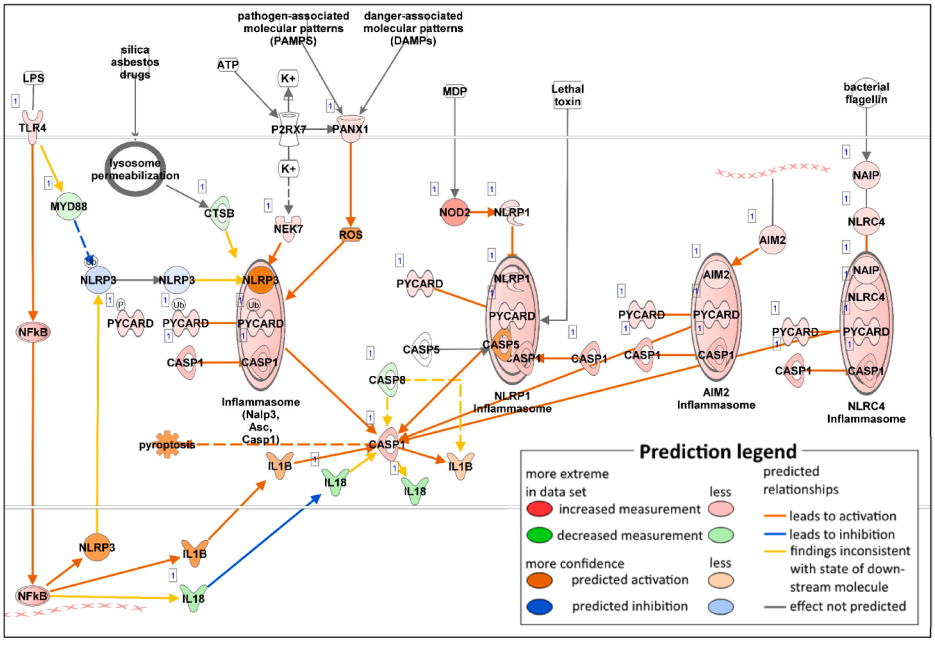

(caption on next page)

Fig. 3. ADP-heptose drives a pro-inflammatory response in intestinal epithelial cells. **(A)** Murine Si organoid monolayer cultures and human colonic organoid monolayer cultures transfected with a TIFA mScarlet2 reporter protein (red), stimulated with and without ADP-H for 8 h (scale bar 100 μm) (6 independent experiments; n = 6). **(B)** Venn diagram comparing differentially regulated genes (p-adjusted < 0.05; $\log_2$(fold change) ± 1) of RNA sequencing from Si organoids stimulated with IL-22 versus mock with Si organoids stimulated with both IL-22 and ADP-heptose (ADP-H) versus mock. **(C)** Selected Gene ontology (biological process) analysis of Si organoids from wild-type mice stimulated with IL-22 combined with ADP-H. **(D)** Comparative transcriptomic plots comparing wild-type Si organoids treated with IL-22 and ADP-H with changes observed in highly inflamed tissue from mice subjected to DSS-induced colitis. Each point represents one transcript. The x-axis represents changes in the colonic transcriptome of highly inflamed mice and the y-axis represents the expression levels of corresponding genes in the colonic transcriptome of Si organoids after IL-22/ADP-H treatment. The red dot represents *Tifa* expression, green dots represent chemokine transcripts, while blue dots represent genes regulated by NF-κB signaling pathway (n = 3/group). **(E)** *CCL20* and *NOS2* gene expression analysis of human organoids treated with IL-22 and ADP-H. *GAPDH* was used for normalization (n = 4). **(F)** Canonical pathway analysis generated by Ingenuity Pathway Analysis (IPA, Qiagen) of wild-type Si organoids treated with IL-22 and ADP-H showing upregulation (red) and predicted activation (orange) of molecules involved in different inflammasomes. Overall data are presented as mean ± SD, and only genes with an adjusted p-value < 0.05 and a $\log_2$(fold change) ± 1 were considered for bioinformatic analysis (n = 3/group). * indicates p < 0.05 by Mann-Whitney test (E).

proficient and −deficient IECs, suggesting that *Tifa* expression alone, in the absence of ADP-heptose, has no overt functions in IECs (Fig. 4**B**). Our comparative approach demonstrates that TIFA expression is strictly required for the responsiveness of IECs to microbial ADP-heptose. Among the 656 genes with a significantly lower expression in TIFA-deficient organoids, we found that pathways activated in IL-22 and ADP-heptose stimulated wild-type Si organoids (Fig. 3**C**) were inhibited in equally stimulated *Tifa*$^{-/-}$ Si organoids, including inflammatory response, immune response, chemotaxis, TNF and NF-κB signaling, and metabolic pathways (Fig. 4**C,** Suppl. Tab. 4). Of note, among the 611 genes with higher expression in ADP-heptose/IL-22 stimulated *Tifa*$^{-/-}$ organoids, pathways linked to host defense where identified (Fig. 4**C**). In particular, we observed elevated expression of Paneth cell-related genes, suggesting that the ADP-heptose-induced suppression of antimicrobial peptides, as observed in **Suppl.** Fig. 2**A**, is strictly TIFA dependent (**Suppl.** Fig. 2**E**). To further validate this observation in complementary approaches, we conducted immunofluorescence staining, Western blot and qPCR analysis for the Paneth cell marker lysozyme. Accordingly, SI organoids from Tifa-proficient and −deficient mice treated with or without ADP-heptose and IL-22 demonstrated that the ADP-heptose-mediated suppression of LYZ expression is functionally dependent on the presence of TIFA in IECs (**Suppl.** Fig. 2**F – H**). Of note, most of the pathways that were differentially regulated between stimulated TIFA-deficient and −proficient Si organoids overlapped with those observed in ADP-heptose-stimulated wild-type organoids (**Suppl**. Fig. 2**I**, Suppl. Tab. 5), further highlighting the essential role of TIFA for epithelial ADP-heptose responsiveness. Notably, *Tifa*$^{-/-}$ mice developed normally and did not exhibit an intestinal pathology under steady-state conditions (**Suppl**. Fig. 3**C – H**), suggesting that in the steady-state gut the ADP-heptose-TIFA signaling axis is not essential for gut development.

Since our pathway analysis revealed that TIFA signaling drives expression of a number of chemokines (Fig. 4**C**), we next investigated the impact of TIFA on chemotaxis. To this end, supernatants from IL to 22 and ADP-heptose stimulated *Tifa*$^{+/+}$- and *Tifa*$^{-/-}$-derived organoids were used to attract wild-type T lymphocytes in a transwell setup. Remarkably, while supernatants from TIFA-proficient organoids were able to attract T cells in a manner similar to CXCL-11, used as a positive control, supernatants obtained from TIFA-deficient organoids attracted T cells to a much lesser extent (Fig. 4**D**), highlighting TIFA as a potential signaling hub between the microbiome and the mucosal immune system. Moreover, our RNA sequencing approach revealed that the T cell-related chemokines *Cxcl11*, *Cxcl16*, *Ccl9*, *Ccl20*, and *Ccl25* were significantly downregulated (**Suppl**. Fig. 2**J**). Moreover, qPCR analysis of *Ccl9* and *Ccl20 expression* clearly showed that the absence of TIFA results in a significant downregulation of these chemokines back to basal expression (**Suppl**. Fig. 2**K**). Furthermore, reduced IEC-specific chemokine production was demonstrated by performing a CXCL2 ELISA using the supernatants previously used in the migration assay. Finally, we observed that organoids from *Tifa*$^{+/+}$ mice produced high levels of CXCL2, whereas this production was abolished in the absence of TIFA (Fig. 4**E**).

TIFA orchestrates an ADP-heptose and NF-κB-dependent inflammatory epithelial response

Different pro-inflammatory signaling pathways have been identified to be involved in the pathogenesis of IBD, including NF-κB signaling,[17] and intestinal microorganisms play a pivotal role in initiating these pathways. As NF-κB signaling was one of the pathways predicted to be induced by stimulation of wild-type organoids with IL-22 and ADP-heptose (Fig. 3**C**), a gene signature that strongly correlated to the signature observed in DSS-induced colitis in mice (Fig. 3**D**), the role of TIFA in mediating activation of the NF-κB signaling pathway was investigated in more detail. While treatment of Si organoids derived from *Tifa*$^{+/+}$ mice with ADP-heptose induced expression of numerous genes related to NF-κB and predicted activation of NF-κB signaling (**Suppl.** Fig. 2**D**), remarkably, this effect was completely abolished in organoids derived from *Tifa* knockout mice (Fig. 4**F**). Moreover, on the protein level, this ADP-heptose-induced activation of the NF-κB pathway in IECs from wild-type organoids, as indicated by increased phosphorylation of p65, was completely abolished in treated Si organoids derived from *Tifa*$^{-/-}$ mice (Fig. 4**G**). In addition, we also detected ADP-heptose-induced activation of the non-canonical NF-κB pathway by Western blotting for p100/p52 in the *Tifa*$^{+/+}$ organoids, which also did not occur in stimulated organoids derived from *Tifa*$^{-/-}$ mice (Fig. 4**G**). To further validate our observation that IL-22 and ADP-heptose stimulation induces inflammasome activation in organoids (Fig. 3**F**), we analyzed expression of Gasdermin D, a hallmark marker of inflammasome activation. Remarkably, while inflammasome activation by cleavage of Gasdermin D was observed in Tifa wild-type organoids stimulated with both IL-22 and ADP-heptose, this effect was completely abolished in Tifa knockout organoids treated in the same way (Fig. 4**H**). Of note, ADP-heptose induced the expression of key inflammasome-related genes in a Tifa-dependent manner (**Suppl**. Fig. 2**L**). Overall, our findings therefore suggest that TIFA-induced NF-κB and inflammasome signaling drive pro-inflammatory gene expression. This observation is consistent with previously published data in gastric cells that identified TIFAsome formation as a potent catalyst of both classical and alternative NF-κB and inflammasome activation.[4–8] .

TIFA is a driver of experimental intestinal inflammation

Given that *Tifa* expression is induced early during intestinal inflammation (Fig. 1**E**), we assessed the function of TIFA in the development of intestinal inflammation using TIFA-deficient mice. To study the effect of TIFA on intestinal inflammation, we challenged littermate *Tifa*$^{+/+}$ and *Tifa*$^{-/-}$ mice with 1.5 % DSS to induce experimental colitis. Interestingly, while DSS-treated wild-type mice developed severe colitis as expected, *Tifa*$^{-/-}$ littermates showed reduced intestinal inflammation, as evidenced by reduced body weight loss (Fig. 5**A**) and reduced shortening of the colon length (Fig. 5**B**), correlated with disease severity. Moreover, *in vivo* endoscopy of the colon revealed a lower endoscopic inflammation score in DSS-treated *Tifa*$^{-/-}$ mice compared to control littermates (Fig. 5**C** and **D**). Furthermore, *Tifa* deficiency was associated

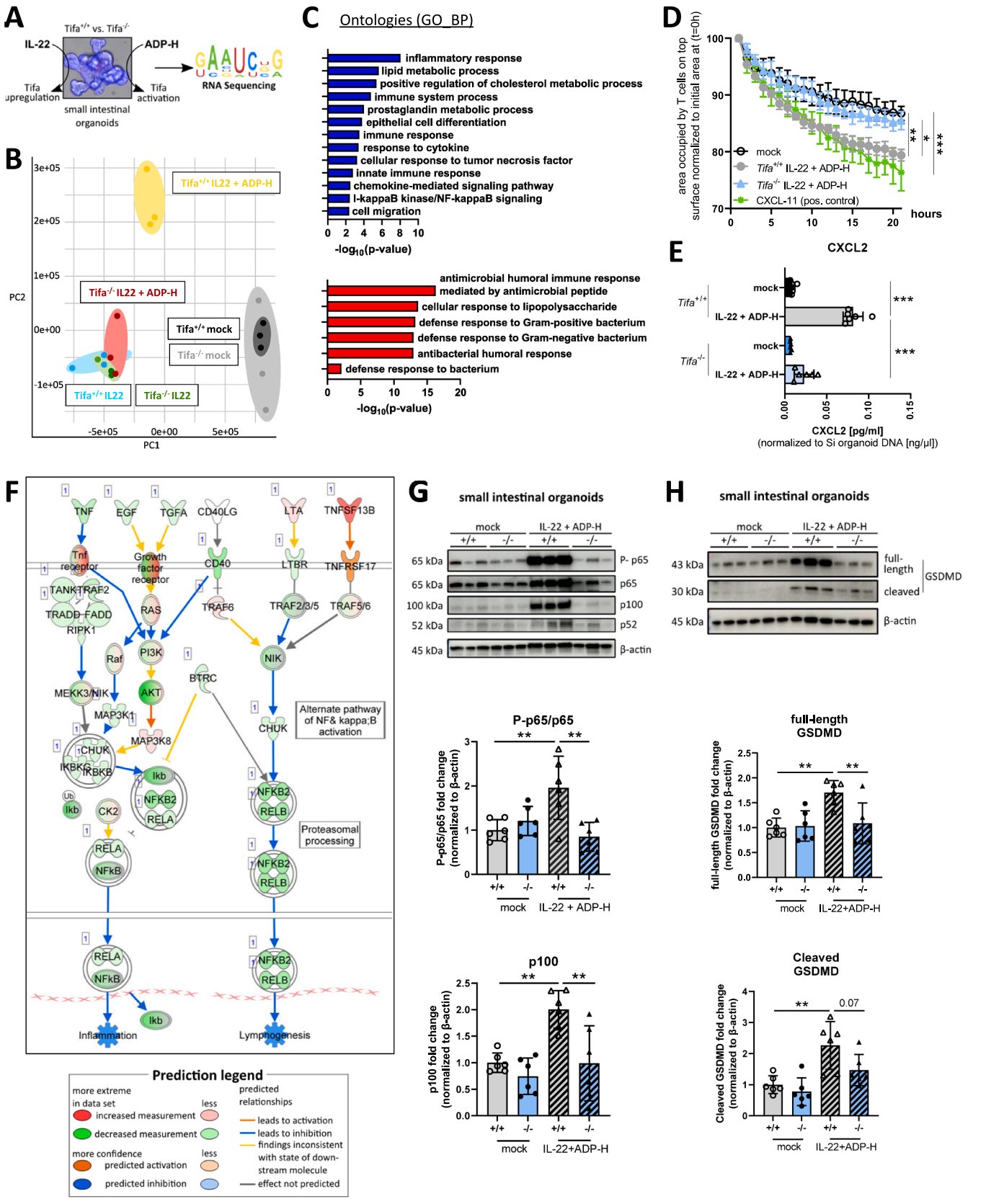

(caption on next page)

Fig. 4. TIFA is essential to orchestrate an (NF-κB-dependent) inflammatory epithelial response. **(A)** Schematic of the RNA sequencing strategy of Si organoids from *Tifa*$^{-/-}$ mice compared to *Tifa*$^{+/+}$ mice, both stimulated with 100 ng/ml murine IL-22 combined with 25 μg/ml ADP-H for 24 h. **(B)** Principal component analysis of the RNA sequencing approach shown in (A). **(C)** Selected Gene ontology biological process (GO_BP) analysis showing selected downregulated (blue) and upregulated (red) pathways from the RNAseq approach shown in (A). **(D)** T lymphocyte migration towards supernatants of unstimulated or with IL-22 and ADP-H stimulated *Tifa*$^{+/+}$ or *Tifa*$^{-/-}$ Si organoids. Cell migration is indicated by the decrease of the occupied area on top of the insert membrane, normalized to the initial area at (t = 0 h). Cxcl-11 diluted in basal culture medium was used as positive control (n = 3/group). **(E)** Quantification of CXCL2 in the supernatant of *Tifa*$^{+/+}$ and *Tifa*$^{-/-}$ Si organoids stimulated with or without IL-22 and ADP-H. Normalization was performed based on the DNA concentration of the organoids (n = 6/group). **(F)** Canonical pathway analysis generated by Ingenuity Pathway Analysis (IPA, Qiagen) of *Tifa*$^{-/-}$ Si organoids treated with IL-22 and ADP-heptose compared to equally treated *Tifa*$^{+/+}$ organoids showing downregulation (green) and predicted inhibition (blue) of molecules involved in the NF-κB signaling pathway. **(G)** Western blot analysis of phospho-p65 (P-p65), p65, NF-κB p100 and p52 of Si organoids from *Tifa*$^{+/+}$ and *Tifa*$^{-/-}$ mice stimulated with or without IL-22 and ADP-H. β-actin was used as loading control (n = 6/group). **(H)** Western blot analysis of Gasdermin D (GSDMD) from Si organoids of *Tifa*$^{+/+}$ and *Tifa*$^{-/-}$ mice stimulated with or without IL-22 and ADP-H. β-actin was used as loading control (n = 6/group). Overall, data are presented as mean ± SD. *, **, and *** indicate $p < 0.05$, $p < 0.01$, and $p < 0.001$, respectively, by one-way ANOVA (Tukey's post hoc test: D, E) or two-way ANOVA (Tukey's correction: G, H).

with reduced histologic signs of colonic tissue destruction as analyzed in H&E sections (Fig. 5**E**) and less epithelial damage as indicated by E-Cadherin staining (Fig. 5**F**). Analysis of the expression of inflammation-related genes, such as *S100a9* and *Il6*, revealed significantly reduced levels in *Tifa* knockout animals (Fig. 5**G**). In addition, *Tifa*$^{-/-}$ mice showed less immune cell infiltration with CD4^{+} T cells, macrophages, and neutrophils after DSS treatment compared to DSS-treated wild-type littermates (Fig. 5**H**). In line with our previously observed *in vitro* findings, inflamed *Tifa*$^{-/-}$ mice showed less activation of the canonical NF-κB signaling pathway, as evidenced by less phosphorylated p65 in Western blot analysis. Notably, in colon tissue of DSS-treated *Tifa*$^{-/-}$ mice, we also observed diminished activation of the non-canonical NF-κB signaling pathway, as indicated by diminished expression of p100 (Fig. 5**I**). Taken together, our results identified TIFA as a driver of experimental intestinal inflammation.

Collectively, our study provides strong evidence that *Tifa* expression is induced by immune-epithelial signaling through the IL-22/STAT3 axis, whereas ALPK1-TIFA signaling and subsequent NF-κB activation is mediated by microbially released ADP-heptose. Taken together, these signaling pathways, linked by TIFA as a central regulator of microbial-epithelial-immune cell communication in IECs, play a key role in intestinal inflammation by influencing NF-κB activation, chemokine production, and inflammasome activation (**graphical abstract**).

In summary, our findings reveal the critical role of TIFA in orchestrating an inflammatory epithelial response to the microbial metabolite ADP-heptose and identify its involvement in the pathogenesis of IBD, implicating it as a potentially promising future target for therapeutic approaches. The interplay between intestinal epithelial TIFA and IL-22 signaling in the context of microbial metabolites implicates that TIFA in IECs is a signaling hub that relays signals from the microbiome to the mucosal immune system. Our finding that TIFA signaling leads to the activation of key inflammatory pathways, including NF-κB, culminating in the production of chemokines that recruit immune cells to the site of inflammation underline this view. Given the current lack of IEC-specific TIFA knockout mice, further research is needed to investigate the cell type-specific role of TIFA during intestinal inflammation and to circumvent the potential limitations of using general TIFA knockout mice. Our data *in vivo* and in primary epithelial cells are in agreement with previous *in vitro* studies using TIFA deficient cell lines. Accordingly, Gaudet *et al.* reported a role for TIFA in surveillance pathways sensing bacterial replication and NF-κB activation in experiments infecting HCT116 and 293 T cells with the pathogen *S. flexneri*.[18] Similarly, Carson *et al.* reported that HELA cells infected with *C. rodentium in vitro* show activation of ALPK1 and TIFAsome formation.[19] Our data extend these previous reports by demonstrating a key role for TIFA at the epithelial barrier *in vivo*. Another novel aspect of our study is the identification of IL-22 signaling through STAT3 as a key inducer of TIFA expression in IECs. We and others have previously shown that IL-22, a cytokine produced by immune cells such as Th17 cells and innate lymphoid cells, plays a protective role in the gut by promoting epithelial barrier function and mucosal healing.[14–15] Our finding that IL-22 induced TIFA signaling promotes an inflammatory response in the epithelium is therefore intriguing. However, the role of IL-22 in intestinal inflammation, particularly in IBD, is complex and context-dependent. For example, IL-22 can also be implicated in pathogenic processes, such as driving cytokine expression[20] also in the context of gut inflammation.[21–22] Our data therefore underline a role of IL-22 in balancing between protective and pro-inflammatory actions within the gut environment. Interestingly, our analyses revealed a previously unknown effect of ADP-heptose on Paneth cells. Specifically, we found that IL-22 and ADP-heptose stimulation significantly reduced Paneth cell numbers – a result that was completely reversed in IECs lacking TIFA. The reasons for this effect are still unclear and require further investigation. However, it can be hypothesized that ADP-heptose may function as a priming agent in IECs, acting as a newly identified modulator of immune responses in the intestine, potentially facilitating bacterial survival, with TIFA in IECs serving as a key mediator of this process.

Methods

Human samples

Human tissue samples were obtained from IBD patients undergoing routine biopsy collection (Suppl. Tab. 6) at the Department of Gastroenterology, Infectious Diseases and Rheumatology of Charité – Universitätsmedizin Berlin and Universitätsklinikum Erlangen. The patients provided written informed consent and the ethics committee of Charité – Universitätsmedizin Berlin or the ethics committee of Universitätsklinikum Erlangen approved the collection of samples. Specimens from healthy and IBD patients were embedded in paraffin and subsequently stained as described below. Data were pseudonymized. The severity of inflammation was assessed using a scale ranging from 0 (no inflammation) to 3 (severe inflammation), in accordance with established criteria from prior publications.[23–24] .

Mice

The generation and maintenance of *Tifa*$^{-/-}$ mice has been described previously (Jackson strain #51101). Mice carrying both loxP-flanked *Stat3* alleles (*Stat3*$^{fl/fl}$) and the Cre-recombinase under the control of the villin promoter (*Stat3*$^{\Delta IEC}$) have been described previously.[14] In addition, *Il22*$^{-/-}$ mice were described before[25] and mice carrying loxP-flanked *Il22ra* alleles[26] were crossed with villin-Cre mice.[27] Germ-free mice were maintained and bred in plastic film isolators (Metall + Plastik GmbH, Radolfzell-Stahringen, Germany). All mice were routinely screened for pathogens according to FELASA guidelines. Animal experiments were performed in accordance with the FELASA welfare regulations. Animal studies were conducted in a sex- and age-matched manner and littermates were used for each experiment, approved by the institutional review board and the ethics committee of the University of Erlangen-Nuremberg and the local animal care committee (Regierung von Unterfranken; animal approval number: 55.2.2–2532-2–1137).

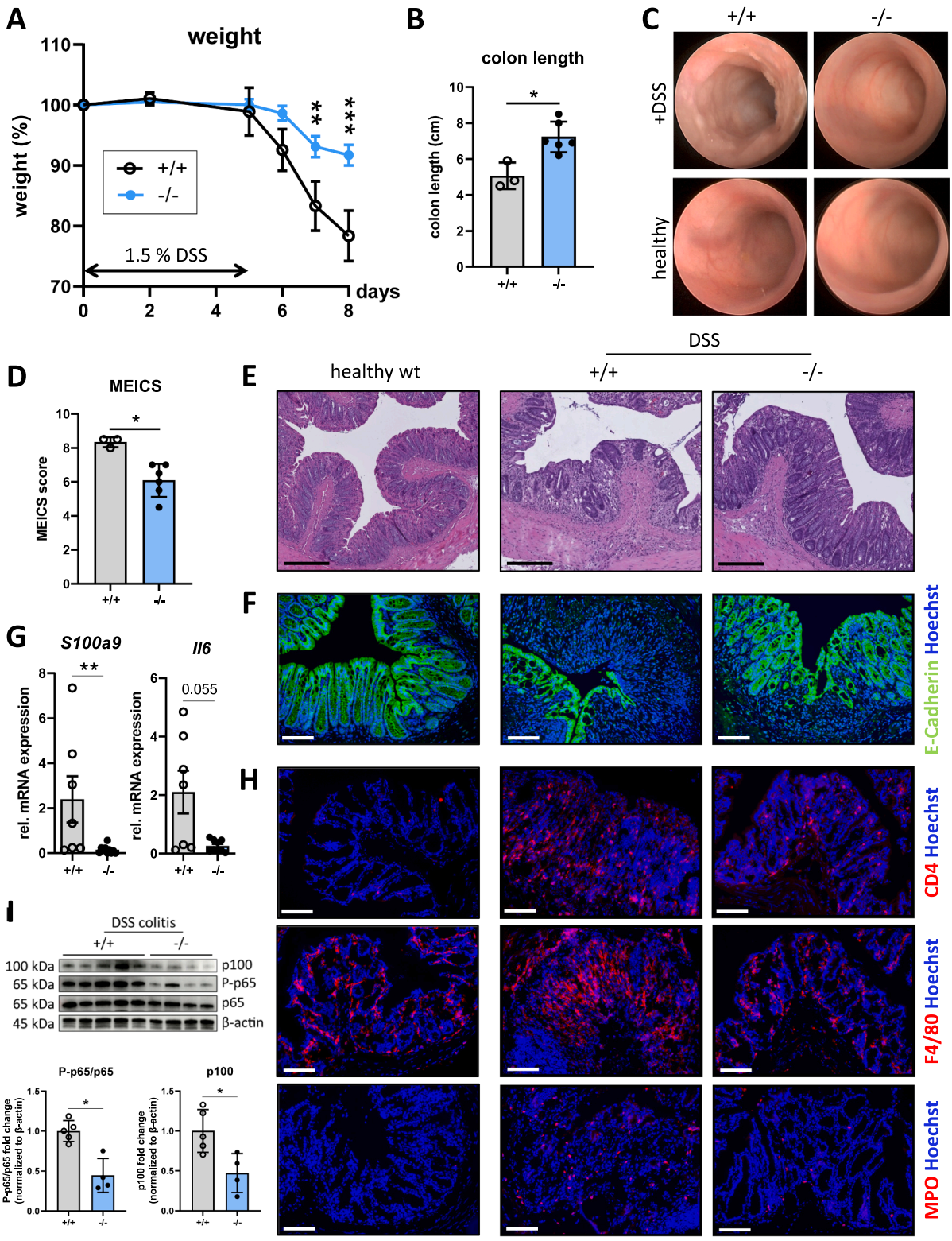

Fig. 5. TIFA is a driver of experimental intestinal inflammation. *Tifa*$^{+/+}$ (n = 7) and *Tifa*$^{-/-}$ mice (n = 9) treated with 1.5 % DSS (2 independent experiments): **(A)** Representative body weight curve, **(B)** colon length measurement, **(C)** endoscopy images, **(D)** murine endoscopic index of colitis severity (MEICS) scoring, **(E)** representative images of hematoxylin and eosin (H&E) staining (scale bar 250 μm), **(F)** immunofluorescence staining for E-Cadherin (scale bar 100 μm), **(G)** gene expression analysis of the inflammatory markers *S100a9* and *Il6*, **(H)** representative immunofluorescence stainings for CD4 (CD4^{+} T cells), F4/80 (macrophages), and MPO (neutrophils) (scale bar 100 μm), **(I)** Western blot analysis of P-p65, p65, and p100. β-actin was used as a loading control (n = 4–5/group). Overall, data are presented as mean ± SD. *, **, and *** indicate $p < 0.05$, $p < 0.01$, and $p < 0.001$, respectively, by one-way ANOVA (Tukey's post hoc test: A) or Mann-Whitney test (B, D, G, I).

DSS-induced colitis model and endoscopy

Intestinal inflammation was induced by oral administration of 1.5 % dextran sulfate sodium (DSS; 36–50 kDa) (MP Biomedicals) in drinking water for the indicated period. Assessment of health status, measurement of weight loss, and evaluation of colitis parameters were performed daily as previously described.[28] Briefly, changes in colonic wall thickening, changes in the normal vascular pattern, presence of fibrin, mucosal granularity, and stool consistency were assessed as colitis parameters by endoscopy. Each parameter was scored with a value from 0 to 3 and the sum of all the five parameters displayed as the murine endoscopic index of colitis severity score (MEICS).

Citrobacter rodentium infection

For *Citrobacter rodentium* infection, the *C. rodentium* strain ICC169 was used as previously described.[29] *C. rodentium* was cultured in sterile LB-media at 37 °C under constant shaking and aeration, supplemented with erythromycin. On day 0, mice were starved for 8 h and then orally gavaged with ~ 10^9 colony forming units (CFU) of *C. rodentium* diluted in 200 µl sterile PBS. Mice were sacrificed on day 8.

Salmonella typhimurium infection

For *Salmonella Typhimurium* infection, the Salmonella enterica serovar Typhimurium strain ΔaroA was used as previously described.[30] *S. typhimurium* was cultured in sterile LB media at 37 °C under constant shaking and aeration, supplemented with streptomycin. One day prior to infection, mice were treated with a single dose of streptomycin by oral gavage. On day 0, mice were starved for 8 h and then orally gavaged with 10^7 – 10^8 CFU of *S. typhimurium* diluted in 200 µl sterile PBS. Mice were sacrificed on day 3.

Helicobacter hepaticus infection

For *Helicobacter hepaticus* infection, mice received 10^8 CFU of *H. hepaticus* (DSMZ, DSMZ no.: 22909) by oral gavage on day 0 and day 1. In addition, mice were injected i.p with an anti-IL-10R blocking antibody (1 mg; clone 1B1.3A; BioXCell) once a week from the day of infection.[31] Mice were sacrificed on day 14 post infection.

Eimeria vermiformis infection

Mice were infected with *Eimeria vermiformis* oocysts (kindly provided by Marc Veldhoen (Instituto de Medicina Molecular, Faculdade de Medicina da Universidade de Lisboa, Portugal)) stored in 2.5 % potassium bichromate as previously described.[32] Briefly, oocysts were prepared by washing three times in deionized water, spinning for 8 min at 1800 g, followed by floating for 10 min at 1100 g, and finally sterilized with sodium hypochlorite. The oocysts were then washed again three times in deionized water and then counted using a Fuchs-Rosenthal chamber. Finally, mice were infected with one thousand oocysts diluted in water by oral gavage. 9 days after oocyst administration, the mice were sacrificed.

IL-22 expression vector

For *in vivo* expression of IL-22, 10 µg/mouse of an IL-22 expression vector was administered by hydrodynamic tail vein injection. This generated minicircle vector contains the mouse α-fetoprotein enhancer and promoter, as well as intronic and polyadenylation signal elements from the mouse albumin gene for long-term expression of IL-22. Constructs containing ORFs for IL-22 were generated in *E. coli*. Empty vectors without IL-22 were used as controls. Mice were sacrificed twelve days after vector administration.

Murine organoid culture

Murine intestinal organoids were established as previously described by Sato *et al.* (Sato et al., 2009). Briefly, mice were sacrificed, and the intestine was removed and cut into small pieces. After incubation in 2 mM EDTA for 30 min, the intestinal epithelial cells were released and filtered through a 70 µm filter. The epithelial cells were then plated in Cultrex (Bio-Techne) and cultured in basal culture medium, changing the medium every 3–4 days and maintaining the organoids in 5 % CO2 at 37 °C and passaged twice a week. Murine organoids were exposed to ADP-heptose (25 µg/ml; InvivoGen), murine IL-22 (100 ng/ml; eBioscience), IL-17A (10 ng/ml; PeproTech), IL-17F (50 ng/ml; PeproTech), IL-21 (50 ng/ml; PeproTech), TNF-a (10 ng/ml; PeproTech), LPS from *Salmonella* (1 µg/ml; Sigma-Aldrich), PGN (10 µg/ml; InvivoGen), CpG (2.55 ng/µl; biomers), Flagellin (10 µg/ml; InvivoGen), MDP (10 µg/ml; InvivoGen), Poly(I:C) (1 µg/ml; InvivoGen), and polarized T-cell supernatants. In all cases, the organoids were stimulated for 24 h.

Human organoid culture

The collection of human material was approved by the local ethics committee. Isolation and culture of human organoids were performed as previously described.[33] Samples were obtained from IBD patients as shown in the table below (Suppl. Tab. 7). Biopsies were cut into small pieces and digested in digestion buffer (DMEM/F-12 (Sigma-Aldrich or Thermo Fisher), 10 mM HEPES (Thermo Fisher), 1x GlutaMAX (Thermo Fisher), 100 U/ml penicillin & 100 µg/ml streptomycin (Thermo Fisher), 100 µg/ml Primocin (InvivoGen), 10 µM Rho kinase inhibitor (STEMCELL Technologies), 5 mg/ml collagenase type II (Sigma-Aldrich)). The digested tissue was then filtered through a 100 µm cell strainer, washed three times in DMEM/F-12 (5 min, 4 °C, 450 g) and plated with Cultrex (Bio-Techne). Organoids were cultured in expansion medium consisting of digestion buffer as described above supplemented with 50 ng/ml human EGF (PeproTech), 100 ng/ml Noggin, 1000 ng/ml R-Spondin-1, 0.5 nM Wnt surrogate (U-Protein Express/ImmunoPrecise Antibodies), 1 µM prostaglandin E2 (Bio-Techne), 0.5 µM ALK5 inhibitor A83-01 (Bio-Techne), 1x B-27 Supplement (Thermo Fisher), 1.25 mM N-acetylcysteine (Sigma-Aldrich), 10 mM nicotinamide (Sigma-Aldrich) and 10 µM p38 inhibitor SB202190 (Sigma-Aldrich) in 5 % CO_2 at 37 °C. After 5 to 7 days of expansion, organoids were disrupted with a syringe and cultured for 7 to 10 days before being used for experiments in expansion medium without Primocin and Rho kinase inhibitor.

Human organoids were exposed to 25 µg/ml ADP-heptose (InvivoGen) and 100 ng/ml human IL-22 (PeproTech) for 24 h.

Organoid monolayer cultures, TIFA plasmid and transfection

Small intestinal organoids were plated as monolayer cultures. Briefly, plates were coated with Matrigel (Corning) diluted 1:30 in PBS for 2 h at 37 °C. Organoids were collected in TrypLE Express Enzyme (Thermo Fisher), incubated for 5 min at 37 °C, and disrupted with a 23G needle. Organoid single cell suspension was plated into coated wells using IntestiCult Organoid Growth Medium (Human) (STEMCELL Technologies) for 2 days. A construct containing the codon optimized full length mouse TIFA c-terminally connected to the sequence of the mScarlet2 reporter protein by a *GGGSGGGSGGGS* linker was constructed and cloned into a eukaryotic expression vector containing the EF-1α core promoter 1 and (R-U5′ sequence of the HTLV Type 1 Long Terminal Repeat 2 (InvivoGen, France)). For transfection of monolayer cultures, 5 µl Lipofectamine 2000 (Thermo Fisher) was mixed with 125 µl Opti-MEM (Gibco), while 2 µg of the described TIFA-mScarlet2 plasmid was mixed with 125 µl Opti-MEM. The TIFA-mScarlet2-Opti-MEM mixture was then added dropwise to the Lipofectamine 2000-Opti-MEM mixture, vortexed, and incubated for 5 min at room temperature. Afterwards, the mixture was added dropwise to the wells and the medium was changed to IntestiCult Organoid Growth Medium

(Human) containing 10 μM Rho kinase inhibitor (STEMCELL Technologies) after 6 h. The next day, 25 μg/ml ADP-heptose (InvivoGen) was added to the wells for 8 h, nuclei were counterstained with Hoechst (1:500; Invitrogen) and actin filaments were stained using Phalloidin (BioLegend).

CXCL2 ELISA

For CXCL2 measurement, small intestinal organoids were stimulated with ADP-heptose (25 μg/ml; InvivoGen) and murine IL-22 (100 ng/ml; eBioscience) for 24 h. The medium was removed, the wells were washed with PBS, and basal culture medium was added. After 24 h, the supernatants were collected. Organoids were collected and DNA was measured for normalization. Quantification of CXCL2 was performed using the Mouse CXCL2/MIP-2 DuoSet ELISA (R&D Systems) according to the manufacturer's recommendations.

Transwell assay

To investigate the influence of IEC-released chemoattractants on cell migration, a transwell assay was performed using the Incucyte SX5® (Sartorius) according to the manufacturer's recommendations. Briefly, Pan T cells were isolated using the Pan T Cell Isolation Kit II, mouse (Miltenyi Biotec). The top insert well of the IncuCyte ClearView plate (Sartorius) was first coated with 20 μg/ml Protein G for 1 h at 37 °C, washed with PBS, and then incubated with 5 μg/ml ICAM-1 for 2 h at 37 °C. Blocking was performed with 1 % BSA in PBS for 30 min in the upper and lower wells. 60,000 isolated Pan T cells were seeded in the coated upper reservoir per well, while supernatants from stimulated organoids were added to the lower reservoir. To obtain organoid supernatants, *Tifa*$^{+/+}$ and *Tifa*$^{-/-}$ Si organoids were stimulated with or without 100 ng/ml IL-22 and 25 μg/ml ADP-H for 24 h. The wells were then washed with PBS, basal culture medium was added for another 48 h, and the supernatants were collected.

T cell polarization

For T cell polarization, naïve CD4^{+} CD25^{-} T cells were isolated using the CD4^{+} T Cell Isolation Kit, mouse (Miltenyi Biotec), followed by the CD25 MicroBead Kit, mouse (Miltenyi Biotec). For polarization of the CD4^{+} CD25^{-} T cells, a 24-well plate was coated with 10 μg/ml anti-CD3 (Bio X-Cell) and 10 μg/ml anti-CD28 (Bio X-Cell), both diluted in PBS, for 1 h at 37 °C. Prior to cell seeding, the wells were washed once with PBS. Th0 activation was performed using RPMI-1640 medium supplemented with 10 % FCS and 1 % penicillin/streptomycin (P/S). Th1 polarization was performed with 5 μg/ml anti-IL-4 (Bio X-Cell) and 20 ng/ml IL-12 (R&D Systems) in RPMI-1640 (+ 10 % FCS, + 1 % P/S). The same medium was used for Th2 polarization together with 5 μg/ml anti-IFNγ (Bio X-Cell), 10 μg/ml anti-IL-12 (Bio X-Cell), 20 ng/ml IL-2 (PeproTech) and 100 ng/ml IL-4 (Immunotools). Treg cells were polarized in RPMI-1640 (+ 10 % FCS, + 1 % P/S) with 5 ng/ml TNFβ (Immunotools) and 20 ng/ml IL-2 (PeproTech). For Th17 polarization, X-Vivo^{TM} 15 (Lonza) media was used supplemented with 5 μg/ml anti-IL4 (Bio X-Cell), 5 μg/ml anti-IFNγ (Bio X-Cell), 100 ng/ml IL-6 (Miltenyi Biotec), 50 ng/ml IL-23 (Miltenyi Biotec), and 20 ng/ml IL-1β (Immunotools). Cells were cultured at 37 °C and 5 % CO_2 for five days.

Histology and immunofluorescence staining

For evaluation of histomorphology, tissue was formalin-fixed and embedded in paraffin. Sections were cut from paraffin blocks and histochemically stained with hematoxylin and eosin. Immunofluorescence staining was performed on formalin-fixed paraffin-embedded sections or cryosections. Cryosections were dried at room temperature for 15 min, then incubated with 4 % PFA at room temperature for 20 min and washed with TBS-T for 5 min. For staining with paraffin-sections, sections were incubated for 1 h at 65 °C, paraffin was removed with ROTI®Histol, and sections were rehydrated in a graded ethanol series. Antigen retrieval was performed in Tris/EDTA buffer for 20 min at 800 W. After cooling down and washing with TBS-T, endogenous biotin-binding sites were blocked with Avidin/Biotin Blocking Kit (Vector Laboratories). For staining of small intestinal organoids, the organoids were plated in chamber slides (ibidi) at a 1:1 dilution in Matrigel. Organoids were fixed with 4 % PFA for 30 min at room temperature and then washed with PBS for 5 min. Permeabilization was performed using 0.3 % Triton-X100 at room temperature for 10 min. Blocking was performed with blocking buffer containing 1 % BSA and 10 % FCS in PBS, incubated for 1 h at room temperature. The following primary antibodies were incubated overnight at 4 °C: E-Cadherin:FITC (1:200; BD Biosciences; #612130), TIFA (1:200; designed by Genscript), Olfm4 (1:300; Cell Signaling; #39141), Lysozyme (1:300; Dako; #A0099), Muc2 (1:500; Novus; #NBP1-31231), Chromogranin A (1:300; Novus; # NB120-15160), Dcamkl1 (1:200; abcam; #ab31704) and Ki67 (1:200; eBioscience; #14–5698-82). The next day, slides were incubated with the appropriate secondary antibody (Alexa Fluor®555 anti-rabbit: 1:400, BioLegend, #406412 for Muc2, ChgA, Dcamkl1, Ki67, Olfm4 and Lysozyme; Biotin anti-rabbit IgG: 1:400, Jackson ImmunoResearch, #111–065-144 combined with Streptavidin DyLight500: 1:400, Thermo Fisher, #84542 for TIFA). Nuclei were counterstained with Hoechst (1:500; Invitrogen), and slides were mounted with fluorescence mounting medium (Dako).

In situ hybridization

RNAScope® (ACDBio) staining was performed on formalin-fixed paraffin-embedded sections according to the manufacturer's instructions. Briefly, sections were incubated for 1 h at 65 °C, paraffin was removed with ROTI®Histol, and sections were incubated in 100 % ethanol. After an air-drying step, the tissue was pretreated with hydrogen peroxide (ACDBio) and then heated at 100 °C for 15 min in Target Retrieval Buffer (ACDBio). After incubation at 40 °C for 30 min in a HybEZ™ Oven (ACDBio) with Protease Plus Reagent (ACDBio) and a wash step, a murine Tifa probe (ACDBio) was applied and incubated at 40 °C for 2 h. Signal amplification and detection were performed using RNAScope® 2.5 HD Red Detection Reagent (ACDBio) according to the manufacturer's instructions. Counterstaining with E-Cadherin:FITC (1:200; BD Biosciences; #612130) for epithelial cells was performed for 2 h at room temperature, and nuclei were detected with Hoechst (1:500; Invitrogen). Finally, the slides were mounted with fluorescence mounting medium (Dako).

Microscopy and quantification of stainings

Bright-field images were obtained using a NanoZoomer 2.0 (Hamamatsu) and fluorescence images were obtained using a DMI 4000B microscope (Leica) with a LEICA DFC360 FX camera. Staining quantification was conducted using ImageJ software. Positive cells per high power field (HPF; 200-fold magnification) were counted, or the signal area of interest was normalized to the corresponding counterstain. For each sample, two to three different images were analyzed, and the average was calculated. The organoid areas were measured for normalization. Villus length and crypt length were measured using ImageJ software.

Western blotting

Organoids were homogenized in M−PER (Thermo Fisher) lysis buffer and tissue in T-PER (Thermo Fisher) lysis buffer, both supplemented with Pierce protease and phosphatase inhibitors (Thermo Fisher) and PMSF (Roche). After incubation at 4 °C for 30 min, the lysates were centrifuged at 14000 rpm for 20 min at 4 °C. Protein concentration was determined by the Bradford assay. After boiling the

samples in LDS sample buffer 4x (Invitrogen) for 5 min at 95 °C, the proteins were separated by SDS-PAGE using Mini-PROTEAN Precast Gels 4–15 % polyacrylamide (Bio-Rad). Proteins were blotted onto PVDF membranes (Bio-Rad) using the TransBlot Turbo Transfer System (Bio-Rad). The following antibodies were incubated overnight at 4 °C: NF-κB p65 (1:1000; Cell Signaling; #3034), Phospho-NF-κB p65 (1:1000; Cell Signaling; #3033), NF-κB2 p100/p52 (1:1000; Cell Signaling; #4882), GSDMD (1:1000; abcam; #ab209845), Lysozyme (1:1000; Dako; #A0099), and HRP Anti-beta Actin (1:10000; abcam; #ab49900). Blots were then incubated with an HRP-conjugated anti-rabbit secondary antibody (1:2500; Cell Signaling; #7074).

RNA Isolation, cDNA transcription and qPCR

Total RNA isolation from tissues or organoids was performed using NucleoSpin® RNA (Macherey Nagel). Synthesis of cDNA was performed using the Script cDNA Synthesis Kit (Jena Bioscience). Gene expression was measured by real-time PCR (Bio-Rad) using SensiFAST SYBR No-ROX (BioCat) and QuantiTect primers (QIAGEN). Gene expression was normalized to the housekeeping genes *Gapdh* or *Hprt*.

mRNA sequencing and analysis

After RNA isolation and QC quality control, samples were sequenced using an Illumina platform (Novogene, Cambridge, UK). We utilized STAR (version 2.7.0d) for mapping to the reference genome (mm10), followed by quantification using feature counts (version 1.6.4). Differential expression analysis of sample groups was conducted employing DESeq2 (version 1.24.0). Enrichment, clustering, and other analyses were performed utilizing a combination of in-house bioinformatic tools and external resources such as Ingenuity Pathway Analysis (IPA; Qiagen) and the Database for Annotation, Visualization, and Integrated Discovery (DAVID) analysis tool. For IPA and DAVID analysis we considered only genes with adjusted p-values less than 0.05 and $\log_2$(-fold change) less than or greater than 1 for analysis. In IPA, the canonical pathway analysis was employed to identify the significant biological pathways. The activation z-score was calculated to predict whether transcriptional regulators are activated or inhibited, utilizing data from published studies available in the Ingenuity knowledge base. Regulators were considered significantly activated if their z-score was above 2 and significantly inhibited if their z-score was below −2. Human transcriptomic cohort data will be available upon acceptance for publication.

Analysis of publicly available datasets

The following publicly available datasets are available under accession codes: GSE92332,[11] GSE190634[12] and E-MTAB-9850.[34] The corresponding raw expression values were log-transformed. Microsoft Excel 2019 was used to sort and compare data, and GraphPad Prism was used to generate graphs.

Statistical analysis

Statistical analysis and graphing were performed using GraphPad Prism8 software. Significance analysis was performed using Mann-Whitney test, one-way ANOVA or two-way ANOVA, as described in the corresponding figure legend. P-values of less than 0.05 (*), 0.01 (**), and 0.001 (***) were considered significant and highly significant. All data are presented as mean ± SD. Most experiments are representative of three independent replicates.

CRediT authorship contribution statement

Lena Erkert: Writing – original draft, Visualization, Project administration, Methodology, Formal analysis, Data curation, Conceptualization. **Barbara Ruder:** Writing – review & editing, Supervision, Data curation, Conceptualization. **Melanie Kabisch:** Methodology. **Reyes Gamez Belmonte:** Writing – review & editing, Supervision, Conceptualization. **Jay V. Patankar:** Writing – review & editing, Supervision. **Miguel Gonzalez Acera:** Visualization, Software, Formal analysis. **Lena Schödel:** Writing – original draft, Visualization, Project administration, Methodology, Formal analysis, Data curation, Conceptualization. **Mircea T. Chiriac:** Writing – review & editing, Resources, Methodology, Conceptualization. **Roodline Cineus:** Resources, Methodology. **Stylianos Gnafakis:** Resources, Methodology. **Tamara Leupold:** Resources, Methodology. **Oana-Maria Thoma:** Writing – review & editing, Resources, Methodology. **Iris Stolzer:** Writing – review & editing, Resources, Methodology. **Astrid Taut:** Methodology. **Veronika Thonn:** Methodology. **Sebastian Zundler:** Resources. **Claudia Günther:** Conceptualization. **Andreas Diefenbach:** Resources. **Anja A. Kühl:** Writing – review & editing, Resources. **Ahmed N. Hegazy:** Writing – review & editing, Resources. **Maximilian Waldner:** Resources. **Marijana Basic:** Resources. **André Bleich:** Resources. **Markus F. Neurath:** Writing – review & editing, Supervision, Funding acquisition. **Stefan Wirt:** Writing – review & editing, Visualization, Supervision, Resources, Funding acquisition, Formal analysis, Conceptualization. **Christoph Becker:** Writing – original draft, Supervision, Resources, Project administration, Funding acquisition, Conceptualization.

Declaration of competing interest

The authors declare that they have no known competing financial interests or personal relationships that could have appeared to influence the work reported in this paper.

Acknowledgements

This work was funded by DFG project TRR241, project number 375876048 (A03, A05, A01, A02, C04, C01, Z03), CRC1181 (C05) and individual grants with project numbers 418055832 and 510624836. The project was also supported by the Interdisciplinary Center for Clinical Research (IZKF: J68, A76, J96, A93). Ahmed N. Hegazy is supported by a Lichtenberg fellowship (Az: 92 087) and a “Corona Crisis and Beyond” grant by the Volkswagen Foundation, a BIH Clinician Scientist grant, the German Research Foundation (375876048-DFG TRR241-A05 and INST 335/597-1), as well as by the ERC-StG “iMOTIONS” grant (101078069).

The authors would like to thank Eva Liebing for substantial proofreading.

Appendix A. The TRR241 IBDome Consortium

Imke Atreya[1], Raja Atreya[1], Petra Bacher[2,3], Christoph Becker[1], Christian Bojarski[4], Nathalie Britzen-Laurent[5], Caroline Bosch-Voskens[6], Hyun-Dong Chang[7], Andreas Diefenbach[8], Claudia Günther[1], Ahmed N. Hegazy[4], Kai Hildner[1], Christoph S. N. Klose[8], Kristina Koop[1], Susanne Krug[4], Anja A. Kühl[4], Moritz Leppkes[1], Rocío López-Posadas[1], Leif S.-H. Ludwig[9,10], Clemens Neufert[1], Markus Neurath[1], Jay V. Patankar[1], Christina Plattner[11], Magdalena Prüß[4], Andreas Radbruch[7], Chiara Romagnani[12], Francesca Ronchi[8], Ashley Sanders[4,10], Alexander Scheffold[2], Jörg-Dieter Schulzke[4], Michael Schumann[4], Sebastian Schürmann[13], Britta Siegmund[4], Michael Stürzl[5], Zlatko Trajanoski[11], Antigoni Triantafyllopoulou[7], Maximilian Waldner[1], Carl Weidinger[4], Stefan Wirtz[1], Sebastian Zundler[1]

[1]Department of Medicine 1, Universitätsklinikum, Friedrich-Alexander-Universität Erlangen-Nürnberg, Erlangen, Germany

[2]Institute of Clinical Molecular Biology, Christian-Albrecht University of Kiel, Kiel, Germany.

[3]Institute of Immunology, Christian-Albrecht University of Kiel and UKSH Schleswig-Holstein, Kiel, Germany.

[4]Charité – Universitätsmedizin Berlin, corporate member of Freie

Universität Berlin and Humboldt-Universität zu Berlin, Department of Gastroenterology, Infectious Diseases and Rheumatology, Berlin, Germany.

[5]Department of Surgery, Universitätsklinikum, Friedrich-Alexander-Universität Erlangen-Nürnberg, Erlangen, Germany.

[6]Department of Dermatology, Universitätsklinikum, Friedrich-Alexander-Universität Erlangen-Nürnberg, Erlangen, Germany.

[7]Deutsches Rheuma-Forschungszentrum, ein Institut der Leibniz-Gemeinschaft, Berlin, Germany.

[8]Charité – Universitätsmedizin Berlin, corporate member of Freie Universität Berlin and Humboldt-Universität zu Berlin, Institute of Microbiology, Infectious Diseases and Immunology.

[9]Berlin Institut für Gesundheitsforschung, Medizinische System Biologie, Charité – Universitätsmedizin Berlin.

[10]Max Delbrück Center für Molekulare Medizin, Charité – Universitätsmedizin Berlin.

[11]Biocenter, Institute of Bioinformatics, Medical University of Innsbruck, Innsbruck, Austria.

[12]Charité – Universitätsmedizin Berlin, corporate member of Freie Universität Berlin and Humboldt-Universität zu Berlin, Institute for Medical Immunology.

[13]Institute of Medical Biotechnology, Friedrich-Alexander University, Erlangen, Germany.

Appendix B. Supplementary material

Supplementary data to this article can be found online at https://doi.org/10.1016/j.mucimm.2025.01.003.

Data availability

Data will be made available on request.

The datasets analyzed during the current study are available in the GEO repository, https://www.ncbi.nlm.nih.gov/geo/query/acc.cgi?acc=GSE92332 and https://www.ncbi.nlm.nih.gov/geo/query/acc.cgi?acc=GSE190634, and the ArrayExpress repository, https://www.ebi.ac.uk/biostudies/arrayexpress/studies/E-MTAB-9850?query=E-MTAB-9850. Transcriptomic data from CD and UC patients, from mouse Tifa$^{-/-}$ tissue and from stimulated organoids will be made publicly available upon publication.

References

1. Coskun M. Intestinal epithelium in inflammatory bowel disease. *Front. Med. (Lausanne)*. 2014;1:24. https://doi.org/10.3389/fmed.2014.00024.
2. Abraham C, Abreu MT, Turner JR. Pattern Recognition Receptor Signaling and Cytokine Networks in Microbial Defenses and Regulation of Intestinal Barriers: Implications for Inflammatory Bowel Disease. *Gastroenterology*. 2022;162:1602–1616.e6. https://doi.org/10.1053/j.gastro.2021.12.288.
3. Li D, Wu M. Pattern recognition receptors in health and diseases. *Signal Transduct Target Ther*. 2021;6:291. https://doi.org/10.1038/s41392-021-00687-0.
4. Zhou P, She Y, Dong N, et al. Alpha-kinase 1 is a cytosolic innate immune receptor for bacterial ADP-heptose. *Nature*. 2018;561:122–126. https://doi.org/10.1038/s41586-018-0433-3.
5. Zimmermann S, Pfannkuch L, Al-Zeer MA, et al. ALPK1- and TIFA-Dependent Innate Immune Response Triggered by the Helicobacter pylori Type IV Secretion System. *Cell Rep*. 2017;20:2384–2395. https://doi.org/10.1016/j.celrep.2017.08.039.
6. Pfannkuch L, Hurwitz R, Traulsen J, et al. ADP heptose, a novel pathogen-associated molecular pattern identified in Helicobacter pylori. *Faseb*. 2019;33:9087–9099. https://doi.org/10.1096/fj.201802555R.
7. Maubach G, Lim MCC, Sokolova O, Backert S, Meyer TF, Naumann M. TIFA has dual functions in Helicobacter pylori-induced classical and alternative NF-κB pathways. *EMBO Rep*. 2021;22. https://doi.org/10.15252/embr.202152878. e52878.
8. Lin T-Y, Wei T-Y-W, Li S, et al. TIFA as a crucial mediator for NLRP3 inflammasome. *PNAS*. 2016;113:15078–15083. https://doi.org/10.1073/pnas.1618773114.
9. Wei T-Y-W, Wu P-Y, Wu T-J, et al. Aurora A and NF-κB Survival pathway drive chemoresistance in acute myeloid leukemia via the TRAF-Interacting Protein TIFA. *Cancer Res*. 2017;77:494–508. https://doi.org/10.1158/0008-5472.CAN-16-1004.
10. Gaudet RG, Sintsova A, Buckwalter CM, et al. INNATE IMMUNITY Cytosolic detection of the bacterial metabolite HBP activates TIFA-dependent innate immunity. *Science*. 2015;348:1251–1255. https://doi.org/10.1126/science.aaa4921.
11. Haber AL, Biton M, Rogel N, et al. A single-cell survey of the small intestinal epithelium. *Nature*. 2017;551:333–339. https://doi.org/10.1038/nature24489.
12. Pavlidis P, Tsakmaki A, Pantazi E, et al. Interleukin-22 regulates neutrophil recruitment in ulcerative colitis and is associated with resistance to ustekinumab therapy. *Nat Commun*. 2022;13:5820. https://doi.org/10.1038/s41467-022-33331-8.
13. Backert I, Koralov SB, Wirtz S, et al. STAT3 Activation in Th17 and Th22 Cells Controls IL-22–Mediated Epithelial Host Defense during Infectious Colitis. *J Immunol*. 2014;193:3779–3791. https://doi.org/10.4049/jimmunol.1303076.
14. Pickert G, Neufert C, Leppkes M, et al. STAT3 links IL-22 signaling in intestinal epithelial cells to mucosal wound healing. *J Exp Med*. 2009;206:1465–1472. https://doi.org/10.1084/jem.20082683.
15. Sugimoto K, Ogawa A, Mizoguchi E, et al. IL-22 ameliorates intestinal inflammation in a mouse model of ulcerative colitis. *J Clin Invest*. 2008;118:534–544. https://doi.org/10.1172/JCI33194.
16. Zenewicz LA, Yancopoulos GD, Valenzuela DM, Murphy AJ, Stevens S, Flavell RA. Innate and adaptive interleukin-22 protects mice from inflammatory bowel disease. *Immunity*. 2008;29:947–957. https://doi.org/10.1016/j.immuni.2008.11.003.
17. Wei J, Feng J. Signaling pathways associated with inflammatory bowel disease. *Recent Pat Inflamm Allergy Drug Discov*. 2010;4:105–117. https://doi.org/10.2174/187221310791163071.
18. Gaudet RG, Guo CX, Molinaro R, et al. Innate Recognition of Intracellular Bacterial Growth Is Driven by the TIFA-Dependent Cytosolic Surveillance Pathway. *Cell Rep*. 2017;19:1418–1430. https://doi.org/10.1016/j.celrep.2017.04.063.
19. Carson D, Barry R, Hopkins EGD, et al. Citrobacter rodentium induces rapid and unique metabolic and inflammatory responses in mice suffering from severe disease. *Cell Microbiol*. 2020;22. https://doi.org/10.1111/cmi.13126. e13126.
20. Arshad T, Mansur F, Palek R, Manzoor S, Liska V. A Double Edged Sword Role of Interleukin-22 in Wound Healing and Tissue Regeneration. *Front Immunol*. 2020;11:2148. https://doi.org/10.3389/fimmu.2020.02148.
21. Andoh A, Zhang Z, Inatomi O, et al. Interleukin-22, a member of the IL-10 subfamily, induces inflammatory responses in colonic subepithelial myofibroblasts. *Gastroenterology*. 2005;129:969–984. https://doi.org/10.1053/j.gastro.2005.06.071.
22. Muñoz M, Heimesaat MM, Danker K, et al. Interleukin (IL)-23 mediates Toxoplasma gondii-induced immunopathology in the gut via matrixmetalloproteinase-2 and IL-22 but independent of IL-17. *J Exp Med*. 2009;206:3047–3059. https://doi.org/10.1084/jem.20090900.
23. Atreya R, Neumann H, Neufert C, et al. In vivo imaging using fluorescent antibodies to tumor necrosis factor predicts therapeutic response in Crohn's disease. *Nat Med*. 2014;20:313–318. https://doi.org/10.1038/nm.3462.
24. Gupta RB, Harpaz N, Itzkowitz S, Hossain S, Matula S, Kornbluth A, Bodian C, Ullman T, Histologic inflammation is a risk factor for progression to colorectal neoplasia in ulcerative colitis: a cohort study, Gastroenterology 133 (2007) 1099-105; quiz 1340-1. Doi: 10.1053/j.gastro.2007.08.001.
25. Zenewicz LA, Yancopoulos GD, Valenzuela DM, Murphy AJ, Karow M, Flavell RA. Interleukin-22 but not interleukin-17 provides protection to hepatocytes during acute liver inflammation. *Immunity*. 2007;27:647–659. https://doi.org/10.1016/j.immuni.2007.07.023.
26. Zheng M, Horne W, McAleer JP, et al. Therapeutic Role of Interleukin 22 in Experimental Intra-abdominal Klebsiella pneumoniae Infection in Mice. *Infect Immun*. 2016;84:782–789. https://doi.org/10.1128/IAI.01268-15.
27. el Marjou F, Janssen K-P, Chang B-H-J, et al. Tissue-specific and inducible Cre-mediated recombination in the gut epithelium. *Genesis*. 2004;39:186–193. https://doi.org/10.1002/gene.20042.
28. Becker C, Fantini MC, Neurath MF. High resolution colonoscopy in live mice. *Nat Protoc*. 2006;1:2900–2904. https://doi.org/10.1038/nprot.2006.446.
29. Riedel CU, Casey PG, Mulcahy H, O'Gara F, Gahan CGM, Hill C. Construction of p16Slux, a novel vector for improved bioluminescent labeling of gram-negative bacteria. *Appl Environ Microbiol*. 2007;73:7092–7095. https://doi.org/10.1128/AEM.01394-07.
30. Grassl GA, Valdez Y, Bergstrom KSB, Vallance BA, Finlay BB. Chronic enteric salmonella infection in mice leads to severe and persistent intestinal fibrosis. *Gastroenterology*. 2008;134:768–780. https://doi.org/10.1053/j.gastro.2007.12.043.
31. Arnold IC, Mathisen S, Schulthess J, Danne C, Hegazy AN, Powrie F. CD11c(+) monocyte/macrophages promote chronic Helicobacter hepaticus-induced intestinal inflammation through the production of IL-23. *Mucosal Immunol*. 2016;9:352–363. https://doi.org/10.1038/mi.2015.65.
32. Figueiredo-Campos P, Ferreira C, Blankenhaus B, Veldhoen M. Eimeria vermiformis Infection Model of Murine Small Intestine. *BioProtoc*. 2018;8. https://doi.org/10.21769/BioProtoc.3122.
33. Pleguezuelos-Manzano C, Puschhof J, van den Brink S, Geurts V, Beumer J, Clevers H. Establishment and Culture of Human Intestinal Organoids Derived from Adult Stem Cells. *Curr Protoc Immunol*. 2020;130:e106.
34. Patankar JV, Müller TM, Kantham S, et al. E-type prostanoid receptor 4 drives resolution of intestinal inflammation by blocking epithelial necroptosis. *Nat Cell Biol*. 2021;23:796–807. https://doi.org/10.1038/s41556-021-00708-8.